Molecules and Cells

Novel Anti-Mesothelin Nanobodies and Recombinant Immunotoxins with *Pseudomonas* Exotoxin Catalytic Domain for Cancer Therapeutics

Minh Quan Nguyen[1], Do Hyung Kim[2], Hye Ji Shim[2], Huynh Kim Khanh Ta[1], Thi Luong Vu[1], Thi Kieu Oanh Nguyen[1], Jung Chae Lim[3], and Han Choe[1,*]

[1]Department of Physiology, University of Ulsan College of Medicine, Asan Medical Center, Seoul 05505, Korea, [2]Elpis-Biotech, Daejeon 35380, Korea, [3]Fatiabgen Co., Ltd., Sejong 30141, Korea
*Correspondence: hchoe@amc.seoul.kr
https://doi.org/10.14348/molcells.2023.0155
www.molcells.org

Recombinant immunotoxins (RITs) are fusion proteins consisting of a targeting domain linked to a toxin, offering a highly specific therapeutic strategy for cancer treatment. In this study, we engineered and characterized RITs aimed at mesothelin, a cell surface glycoprotein overexpressed in various malignancies. Through an extensive screening of a large nanobody library, four mesothelin-specific nanobodies were selected and genetically fused to a truncated *Pseudomonas* exotoxin (PE24B). Various optimizations, including the incorporation of furin cleavage sites, maltose-binding protein tags, and tobacco etch virus protease cleavage sites, were implemented to improve protein expression, solubility, and purification. The RITs were successfully overexpressed in *Escherichia coli*, achieving high solubility and purity post-purification. *In vitro* cytotoxicity assays on gastric carcinoma cell lines NCI-N87 and AGS revealed that Meso(Nb2)-PE24B demonstrated the highest cytotoxic efficacy, warranting further characterization. This RIT also displayed selective binding to human and monkey mesothelins but not to mouse mesothelin. The competitive binding assays between different RIT constructs revealed significant alterations in IC_{50} values, emphasizing the importance of nanobody specificity. Finally, a modification in the endoplasmic reticulum retention signal at the C-terminus further augmented its cytotoxic activity. Our findings offer valuable insights into the design and optimization of RITs, showcasing the potential of Meso(Nb2)-PE24B as a promising therapeutic candidate for targeted cancer treatment.

Keywords: cancer therapeutics, cytotoxic efficacy, mesothelin-targeting, nanobody-based recombinant immunotoxin, PE24B

INTRODUCTION

Mesothelin, a glycosylphosphatidylinositol (GPI)-anchored cell surface protein, emerges as a pivotal biomarker owing to its selective overexpression in a variety of human cancers, including mesothelioma, ovarian cancer, pancreatic adenocarcinoma (Hassan and Ho, 2008), lung adenocarcinoma (Ho et al., 2007), gastric adenocarcinoma (Han et al., 2017), and cholangiocarcinoma (Yu et al., 2010). This protein interacts with MUC16 (commonly referred to as CA125), suggesting that the mesothelin–MUC16 interaction plays a significant role in tumor implantation and peritoneal dissemination through enhanced cellular adhesion (Rump et al., 2004). Initially identified in OVCAR-3 human ovarian carcinoma cells, the mesothelin gene (Meso) is located on chromosome 16p13.3 (Chang and Pastan, 1996; Chang et al., 1992). The gene en-

Received September 21, 2023; revised October 10, 2023; accepted October 17, 2023; published online December 1, 2023

eISSN: 0219-1032

codes a precursor molecule called pre-pro mesothelin, which undergoes proteolytic cleavage to produce two functionally distinct entities: a 31 kDa megakaryocyte-potentiating factor and the 40 kDa GPI-anchored mesothelin protein (Chang and Pastan, 1996).

Targeted cancer therapies such as immunotoxins represent a revolutionary shift in oncological treatments, aiming to reduce collateral damage to normal tissues (Alewine et al., 2015; Allahyari et al., 2017; Wolf and Elsasser-Beile, 2009). Recombinant Immunotoxins (RITs) amalgamate the toxin fragment with either the Fv or Fab segment of an antibody or a cytokine, offering exquisite specificity for cancer cell eradication (Bird et al., 1988; Huston et al., 1988). The translation of mesothelin-targeting immunotoxins from bench to bedside has encountered an array of challenges. Earlier iterations such as SS1P, which represents a mesothelin-targeting antibody fragment genetically fused with a truncated segment of *Pseudomonas* exotoxin A (PE), demonstrated robust anti-cancer activities but elicited immune responses that compromised their therapeutic potential (Kreitman et al., 2009). Identification and silencing of human B-cell epitopes within PE led to the derivation of PE24B, a toxin variant characterized by reduced immunogenicity and antigenicity (Liu et al., 2012). Subsequent innovations led to more refined versions like LMB-100, which showed improved efficacy and reduced immunogenicity (Alewine et al., 2014; Zhang et al., 2017). However, the quest for an ideal RIT continues, with current efforts focusing on improving drug delivery efficiency, managing immunogenicity, and optimizing cost-effectiveness (Cerise et al., 2019; Jiang et al., 2020; Kreitman et al., 2009).

Nanobodies, representing the functional variable regions of camelid heavy-chain-only antibodies, have garnered attention due to their high specificity, stability, small size, and ease of production (Xiang et al., 2021). They have been employed in a multitude of applications, from brain delivery and imaging to drug development (Keyaerts et al., 2016; Khaleghi et al., 2017; Prantner et al., 2018; Roovers et al., 2007; Roovers et al., 2011; Ruiz-Lopez and Schuhmacher, 2021; Shahbazi-Gahrouei and Abdolahi, 2013; Wouters et al., 2020).

In the present investigation, we undertook a comprehensive screening of a nanobody library specifically targeting mesothelin with the objective of identifying novel mesothelin-binding nanobodies. Subsequently, we engineered nanobody-based RITs by fusing these novel nanobodies with PE24B. We assessed the cytotoxic potential and cellular internalization dynamics of the engineered RITs across several cancer cell lines. Additionally, we conducted evaluations to determine the RIT's cross-species reactivity.

MATERIALS AND METHODS

Materials

All chemicals were analytical grade or cell-culture grade. Dithiothreitol and isopropyl-β-D-thiogalactopyranoside (IPTG) were from Anaspec (USA). Ampicillin and gentamicin were from Duchefa Biochemie (The Netherlands). NaCl, glycerol, sodium cyanoborohydride, and sodium phosphate dibasic were from Samchun Chemical (Korea). Coomassie brilliant blue R-250 and Tris-HCl were from Amresco (USA). Ammonium bicarbonate was from Junsei Chemical (Japan). Imidazole was from Daejung Chemicals (Korea). The cell counting kit-8 (CCK-8) was from Dojindo (USA). Dulbecco's modified Eagle medium (DMEM), Roswell Park Memorial Institute (RPMI) 1640 medium, 0.25% trypsin-ethylenediaminetetraacetic acid (EDTA), fetal bovine serum (FBS), G418, and penicillin-streptomycin (P/S) were from Gibco (USA). TRIzol was from Cosmogenetech (Korea). The Reverse Transcription Premix kit was from Elpis-Biotech (Korea). The human mesothelin (296-580 aa of Uniprot Q13421-3) for nanobody library screening was from Acrobiosystems (USA). The anti-His fluorescein isothiocyanate (FITC) secondary antibody was from Abcam (UK). The PE24B and tobacco etch virus (TEV) protease were produced in house, as described in previous publications (Do et al., 2014; Lee et al., 2019; Nguyen et al., 2014; Song et al., 2013).

The AGS and NCI-N87 cell lines were obtained from the Korean Cell Line Bank (Korea). The HL60 cell line was a gift from Dr. Chan Jung Park. The ExpiHEK293F cell line and Expi293 Expression Medium were from Thermo Fisher Scientific (USA). Lobstr *Escherichia coli* was from Kerafast (USA). The CO_2 shaking incubator was from N-Biotek (Korea).

All chromatography columns (ÄKTA Prime, ÄKTA Start, and the ÄKTA Go protein purification system) were from GE Healthcare (USA). The 0.45 μm pore size filter was from Hyundai Micron (Korea). The dialysis membranes were from Viskase (USA). The Amicon Ultra concentrators were from Merck Millipore (USA). The Acrodisc syringe filters were from Pall South Korea (Korea). The SRT-C SEC 300 column was from Sepax (USA). The CELENA X High Content Imaging System was from Logos Biosystems (Korea).

Screening of the nanobody library

The nanobody library screening was carried out using an in-house nanobody library (5.02×10^{10} cell population). Briefly, the process of screening against human mesothelin (E296-G580 of Uniprot Q13421-3) was executed through conventional phage display panning (bio-panning) with slight modifications, including three to four rounds of panning for enriching the Meso-specific nanobody library. Phages were applied to mesothelin-coated wells, washed extensively, eluted, and amplified for multiple rounds of panning, each involving various solutions and temperature-controlled incubations, and then prepared by precipitation. After the final round of panning, analysis of the phages' binding to the target was performed using an enzyme-linked immunosorbent assay (ELISA) with incubations involving various reagents, including the chromogenic substrate tetramethylbenzidine for signal development. Specific individual clones were selected through dilution, inoculation, and lysis, followed by further testing for specific binding to the antigen using the phage ELISA method as mentioned.

Construction of Meso(Nb)-PE24B fusion protein for *E. coli* expression

The construction of the mesothelin nanobody immunotoxin fused to PE24B was carried out using Gibson Assembly. Specifically, the expression vector, Meso(Nb)-PE24B, was designed for optimal expression in the *E. coli* system. Inserts,

namely TEVrs-Meso(Nb)-Furin and Furin-PE24B, were engineered to contain 15-20 base pairs of homology with the flanking regions of the insertion site in the vector backbone, as illustrated in Supplementary Fig. S1. These inserts were polymerase chain reaction (PCR)-amplified using tailored primers to facilitate precise insertion. The assembled DNA constructs were then introduced into *E. coli* DH5α cells via heat-shock transformation. Clones containing the intended construct were identified through ampicillin-resistance screening and subsequently verified by DNA sequencing.

Construction of Meso(Nb2) variants

The construction of Meso(Nb2) expression vectors tailored for the *E. coli* expression system was accomplished via *in vivo* DNA cloning techniques. Both target genes and the linearized vector backbone were PCR-amplified utilizing sequence-specific primers. The resulting amplicons were designed to contain 15-40 base pairs of homologous sequences at their ends to facilitate precise *in vivo* recombination. For bacterial transformation, *E. coli* IVEC3 cells were cultured overnight in 1.5 ml Eppendorf tubes at 37°C for a period of 16-24 h. Post-culturing, the tubes were chilled on ice for 5-10 min. Cells were then harvested by centrifugation at 5,000 × *g* for a 1-min duration. The PCR-amplified insert and linear vector were mixed with 100 μl of ice-cold TSS (transformation and stock solution) to form the TSS-DNA solution. This mixture was immediately added to the chilled IVEC3 cells and flash-frozen in liquid nitrogen. Subsequently, the frozen tubes were thawed on ice for a 10-min incubation, followed by a brief vortexing step. To facilitate cell recovery, 1 ml of L broth was added, and the tube was incubated at 37°C for an additional 45 min. Post-incubation, cells were harvested by centrifugation at 5,000 × *g* for 1 min and spread on agar plates containing appropriate antibiotics for selection. Successfully transformed colonies were initially screened for ampicillin resistance. Furthermore, the presence of the target gene insert in the expression vector was verified through colony PCR, yielding the expected size for the target band. Final confirmation of the successfully assembled vectors was obtained by DNA sequencing.

Expression and solubility of proteins in lobstr *E. coli*

The plasmid harboring the target gene was transformed into Lobstr *E. coli* cells, followed by selection for antibiotic resistance to identify successful transformants. Colonies were screened for robust protein expression by initially growing them on LB agar plates supplemented with 100 μg/ml ampicillin. The promising colonies were then inoculated into liquid LB media containing the same antibiotic concentration, followed by overnight incubation at 37°C and shaking at 200 rpm. The overnight culture was subsequently diluted 1:100 into 2 L of fresh LB media, again fortified with the appropriate antibiotics. Cells were incubated at 37°C with a shaking speed of 200 rpm until the optical density at 600 nm reached a range of 0.5-0.6. At this point, IPTG was added to a final concentration of 0.5 mM to trigger recombinant protein expression. The culture was then shifted to 18°C and allowed to incubate for an additional 18 h at 200 rpm to optimize protein solubility. Following incubation, cells were harvested by centrifugation at 5,000 × *g* for 30 min at 4°C. The resultant cell pellets, approximately 1 ml in volume, were subsequently subjected to lysis via ultrasonic disruption on ice. The sonication protocol involved 5-s bursts with 5-s intervals, all in the presence of a sonication buffer comprising 20 mM Tris-HCl, 5% (v/v) glycerol, and adjusted to pH 8.0. The lysate was clarified by further centrifugation at 17,000 × *g* for 10 min at 4°C, enabling the separation of soluble and insoluble cellular fractions.

Protein expression levels and solubility were assessed by running the samples on a 10% tricine SDS-PAGE gel. Quantitative analysis was performed using Gel Analyzer 19.1 software, and the expression and purity levels of the target proteins were calculated using the following equations:

$$\text{Expression level} = F/I$$
$$\text{Solubility level} = S/(S + P)$$

where F is the amount of fusion protein, I is the total cellular protein amount after IPTG induction, S is the amount of fusion protein in the supernatant, and P is the amount of the fusion protein in the pellet.

Purification of Meso(Nb)-PE24B and Meso(Nb2) variants

After 18 h of induction with 0.5 mM IPTG and 100 μg/ml ampicillin at 18°C, 500 ml of bacterial culture in the Lobstr strain was harvested via centrifugation at 3,800 × *g* for 30 min at 4°C (Hyun et al., 2021; Kim et al., 2022). The resulting cell pellets were either processed immediately or stored at −20°C for future use. The bacterial cell pellets were resuspended in 80 ml of buffer A, which consisted of 20 mM Tris-HCl at pH 8.0 and 5% (v/v) glycerol. Cell lysis was achieved through sonication using an ultrasonic cell disruptor. Subsequently, the cell lysates were clarified by centrifugation at 23,000 × *g* for 20 min at 4°C. The clarified supernatant was then passed through a 0.45 μm membrane filter for additional purification. To prepare the supernatant for chromatography, sodium chloride was added to achieve a concentration of 0.3 M. The prepared supernatant was subsequently loaded onto an MBPTrap HP column for affinity purification. The eluted MBP-Meso(Nb2)-PE24B fusion protein fractions, obtained using 25 mM maltose, were dialyzed back into buffer A. TEV protease was then added at a ratio of either 1:50 or 1:20 to cleave the fusion tag. Following the protease treatment, the target protein Meso(Nb2)-PE24B pool was salt-adjusted to 0.5 M NaCl and subjected to a second round of purification using a HisTrap HP column. Finally, the purified protein was desalted into buffer A using a desalting column. To evaluate the success of each purification step, the samples were analyzed using 10% tricine SDS-PAGE gels. Protein concentrations were quantified through BCA assays, employing bovine serum albumin as a standard for calibration.

Cell culture conditions and maintenance

The cell lines used in this study were cultured as per protocols from either the American Type Culture Collection or the Korea Cell Line Bank. The MIA PACA-2 cell line was maintained in DMEM containing 10% FBS and 1% P/S. For mesothelin-transfected MIA PACA-2 cells, the culture medium was identical but also included 50 μg/ml G-418 for selective pressure. ExpiHEK293F cells, used for the expression and purifica-

tion of all recombinant mesothelin variants, were cultivated in Expi293 Expression Medium. The AGS, NCI-N87, and HL60 cell lines were cultured in RPMI 1640 medium, also supplemented with 10% FBS and 1% P/S. To maintain experimental consistency, all cell lines were restricted to fewer than 10 passages, while the mesothelin-transfected MIA PACA-2 cells were used at fewer than 5 passages.

Expression and purification of human, monkey, and mouse mesothelins

To express and purify various forms of mesothelin, genes corresponding to specific residues of human, monkey, and mouse mesothelin, as well as human SMRP and truncated mesothelin forms, were subcloned into the pcDNA3.4 mammalian expression vector. The detailed UniProt IDs and residue ranges for these constructs are as follows: human mesothelin (E296-L597, UniProt Q13421-3), mouse mesothelin (E300-S600, UniProt Q61468-1), and monkey mesothelin (D296-S598, UniProt F6Q1U7).

Expi-HEK293F cells were cultured and transfected following the manufacturer's guidelines. Specifically, a 100 ml culture at a density of 3×10^6 cells/ml was transfected using preformed Expifectamine:DNA complexes at a final concentration of 1 μg/ml. Cells were incubated at 37°C and 8% CO_2, with shaking at 125 RPM, in 500 ml Erlenmeyer flasks using a CO_2 shaking incubator. Expression enhancers were added 18-20 h post-transfection, in line with the manufacturer's recommendations, and the culture was continued under the same conditions until harvest at day 5 post-transfection.

For protein purification, immobilized metal affinity chromatography (IMAC) was carried out using an AKTA Go protein purification system. The culture supernatant was loaded onto a pre-equilibrated 5 ml HisTrap FF column with 10 mM imidazole. Following elution, fractions were analyzed via non-reducing and reducing SDS-PAGE and stained with Coomassie Brilliant Blue R-250. Fractions enriched in mesothelin were combined and dialyzed against Dulbecco's phosphate-buffered saline (PBS). Protein concentrations were assessed spectrophotometrically at 280 nm using their respective molar extinction coefficients, and the purity of the recombinant proteins was further verified using size-exclusion chromatography on an SRT-C SEC 300 column.

Establishment of stable MIA PaCa-2 cell lines expressing human, mouse, and monkey mesothelin

For the generation of stable cell lines expressing various forms of mesothelin, MIA PaCa-2 cells were transfected with a pcDNA3.1 expression vector containing the cDNA sequences for human, mouse, and monkey mesothelin. Post-transfection, cells were cultured in medium supplemented with 500 μg/ml of G418 to select for stably transfected cells. Individual clones that demonstrated resistance to G-418 were subsequently isolated and expanded for further characterization and experimentation.

Assessment of cross-species reactivity of mesothelin isoforms using ELISA

For the evaluation of cross-species reactivity, 96-well microtiter plates were coated with 100 ng/100 μl of various purified mesothelin proteins—mouse mesothelin, monkey mesothelin, and human mesothelin—dissolved in coating buffer. Plates were sealed with adhesive plate sealers and incubated overnight at 4°C to allow for optimal protein adsorption. Following the overnight incubation, the plates were washed thrice using 1× PBS to remove any unbound proteins. Next, 100 μl of a three-fold serial dilution of each test antibody—PE24B-His, Meso(Nb)-PE24B, and Meso(Nb)-PE24B-His—starting from a concentration of 200 nM and diluted 1:500 in assay-specific dilution buffer, was added to the wells. Plates were resealed and incubated for 1 h at 37°C to facilitate antibody binding. Post primary antibody incubation, the wells were washed three times with 1× PBS to remove unbound antibodies. A 100 μl aliquot of anti-*Pseudomonas* exotoxin A secondary antibody, diluted 1:10,000 in assay-specific buffer, was added to each well. The plates were again sealed and incubated for 1 h at 37°C. Upon completion of secondary antibody incubation, the plates were washed thrice with 1× PBS. Detection was carried out by adding 100 μl of horseradish peroxidase–conjugated anti-rabbit antibody at a dilution of 1:1,000. Plates were incubated for an additional 1 h at 37°C. After the final antibody incubation, the plates were washed with 1× PBS, and 100 μl of tetramethylbenzidine substrate was added to each well. Plates were incubated for 3 min at room temperature in the dark to develop the color. The reaction was quenched by the addition of 100 μl of 2 M sulfuric acid stop solution to each well. Absorbance values were then quantified at 450 nm using a microplate reader to assess the cross-species reactivity of the mesothelin isoforms.

Evaluating species-specific mesothelin reactivity using flow cytometry

To assess the cross-reactivity of the mesothelin isoforms across species, MIA PACA-2 cells expressing species-specific variants of mesothelin were prepared. Cells were first dissociated using a solution containing 0.25% trypsin and 0.53 mM EDTA, and the incubated for 5 min at 37°C to facilitate detachment. After detachment, the cells were resuspended and stained using a 3-fold serial dilution starting from a concentration of 1,000 nM of various probes: PE24B, Meso(Nb2), and Meso(Nb2)-PE24B-His. Staining was performed in FACS (fluorescence-activated cell sorting) buffer, and the mixture was incubated for 30 min at 4°C to enable optimal binding of the probes to the mesothelin antigens. Subsequently, the cells were washed thoroughly with cold 1× PBS to remove any unbound or excess probes. The cells were then exposed to an anti-His FITC-conjugated secondary antibody at a dilution of 1:500. This mixture was further incubated for 30 min at 4°C to allow specific binding of the secondary antibody to the His-tagged probes. Finally, the stained and treated single-cell suspension was analyzed using a CytoFLEX flow cytometer. The data collected facilitated the evaluation of species-specific reactivity and binding affinity of the various mesothelin isoforms.

Internalization of Meso(Nb2)-FP in pancreatic and gastric cancer cell lines using high-content imaging

The MIA/Meso-10 and NCI-N87 cell lines were initially dissociated using a 0.25% trypsin and 0.53 mM EDTA solution. A

5-min incubation at 37°C was carried out to ensure complete cellular dissociation. The dissociated cells were then seeded in 24-well plates at a density of 1×10^5 cells per well and cultured overnight at 37°C in complete growth media to permit adequate cellular adherence and expansion. Post-adherence, the cells were rinsed with sterile 1× PBS to eliminate any remaining media or cellular byproducts. Subsequently, the cells were exposed to 100 μg/ml of Meso(Nb2)-FP conjugated antibodies. The incubation was performed for various durations: 2 h, 4 h, or overnight. The incubation medium was DMEM/RPMI enriched with 3% FBS, 0.5% bovine serum albumin, and 1× PBS. Upon completion of the designated incubation times, cells were washed with 1× PBS to remove any non-internalized antibodies. The rate and extent of antibody internalization were then assessed either at 2-h intervals or continuously overnight, utilizing the CELENA X High Content Imaging System.

Quantitative assessment of cell viability following treatment with Meso(Nb)-PE24B and its variants using CCK-8 assay

Adherent cells from various lines (AGS, MIA PACA-2, NCI-N87, and HL60) were first dissociated using a trypsin-EDTA solution (0.25% trypsin, 0.53 mM EDTA), followed by a 5-min incubation at 37°C to ensure complete dissociation. A seeding density of 3,000 to 5,000 viable single cells was plated into each well of a 96-well plate. Following a 24-h incubation period at 37°C to facilitate cell attachment, the cells were treated with incremental concentrations (0.001, 0.01, 0.1, 1, 10, 100, and 1,000 nM) of Meso(Nbs)-PE24B, its variants (Meso(Nb2)), or PE24B alone, diluted in complete culture media. Cell viability was subsequently measured using the CCK-8 assay. For the AGS cell line, assessments were made 2 days post-treatment, whereas for the NCI-N87 cell line, the evaluation was conducted 3 days post-treatment. In complementary experiments involving the AGS, MIA PACA-2, and HL60 cell lines, assessments were performed after 3 days; for the NCI-N87 cell line, after 4 days. To perform the CCK-8 assay, 10 μl of CCK-8 solution was added to each well. Optical density readings were taken between 1 to 4 h post-addition at an absorbance wavelength of 450 nm. The blank control comprised complete media augmented with 10 μl of CCK-8 solution. Each protein concentration was tested in triplicate to ensure data reliability.

The cell viability data were analyzed using the Hill equation:

$$Y = Top - (Top-Bottom)/(1 + (IC_{50}/X)^{HE})$$

where Y represents cell viability, Top is the maximal observed cell viability, Bottom signifies the minimal cell viability, IC_{50} indicates the agonist concentration yielding a response midway between Top and Bottom, X is the agonist concentration at each data point, and HE stands for the Hill coefficient. Data analyses were carried out using Microsoft Excel 2016 (Microsoft, USA).

Statistical analysis and data presentation

For robust statistical evaluation, all experimental data are reported as mean ± SEM, with a sample size (n) of three or greater, based on triplicates from at least three independent biological replicates. The statistical software Prism 8 (GraphPad Software, USA) was employed for all analyses. The level of significance was set at $P \leq 0.05$.

RESULTS

Design and synthesis of targeted immunotoxin genes

We identified four mesothelin (Meso)-specific nanobodies via a comprehensive screening process utilizing a nanobody library encompassing 5.02×10^{10} distinct cell populations (data not shown). These selected nanobodies were subsequently genetically engineered to create fusion constructs with the N-terminal end of a truncated variant of *Pseudomonas* exotoxin, termed PE24B (Fig. 1A). To permit site-specific proteolytic cleavage by the cellular protease furin, we strategically introduced a furin-sensitive cleavage site between the nanobody and the toxin domains. To enhance both the expression yield and solubility of the resultant fusion proteins, we incorporated a maltose-binding protein (MBP) domain at the N-terminus. Moreover, to facilitate the seamless removal of the MBP tag during the subsequent purification steps, a cleavage site for TEV protease was integrated between the MBP domain and the nanobodies. The genes encoding these immunotoxins were synthesized through either Gibson Assembly or *in vivo* DNA cloning methodologies (Supplementary Fig. S1).

Expression and solubility profiling of RITs

The RITs were heterologously overexpressed in the *E. coli* strain Lobstr under controlled conditions at 18°C. Quantitative analyses of both expression and solubility were conducted using SDS-PAGE. The proteins exhibited expression levels ranging between 50%-60%, with a notably high solubility exceeding 95% (Fig. 1B, Table 1).

Purification strategy for RITs

Recombinant proteins were isolated from 500 ml bacterial cultures utilizing a two-step affinity chromatography protocol, incorporating both dextrin-based and IMAC columns. During these purification stages, the N-terminal MBP tags were enzymatically cleaved via the action of TEV proteases. Subsequent analyses confirmed the isolated proteins were highly pure, with purity exceeding 95% (Fig. 1C, Table 2).

Evaluation of cytotoxic potency of mesothelin-targeted RITs

We investigated mesothelin expression across various cell lines utilizing quantitative PCR (Supplementary Fig. S2, Supplementary Methods). Notably, NCI-N87 cells exhibited the highest mesothelin expression levels, while both HL60 cells demonstrated relatively minimal expression. Cytotoxic efficacies of the four purified RITs were assessed through their application to NCI-N87, AGS, and HL60 cell lines over a 72-h incubation period. Among the RITs, Meso(Nb2)-PE24B exhibited the most potent cytotoxic activity, followed by Meso(Nb11)-PE24B, in both NCI-N87 and AGS gastric carcinoma cell lines (Figs. 2A and 2B, Table 3). These cell lines displayed greater viability than the negative control at low

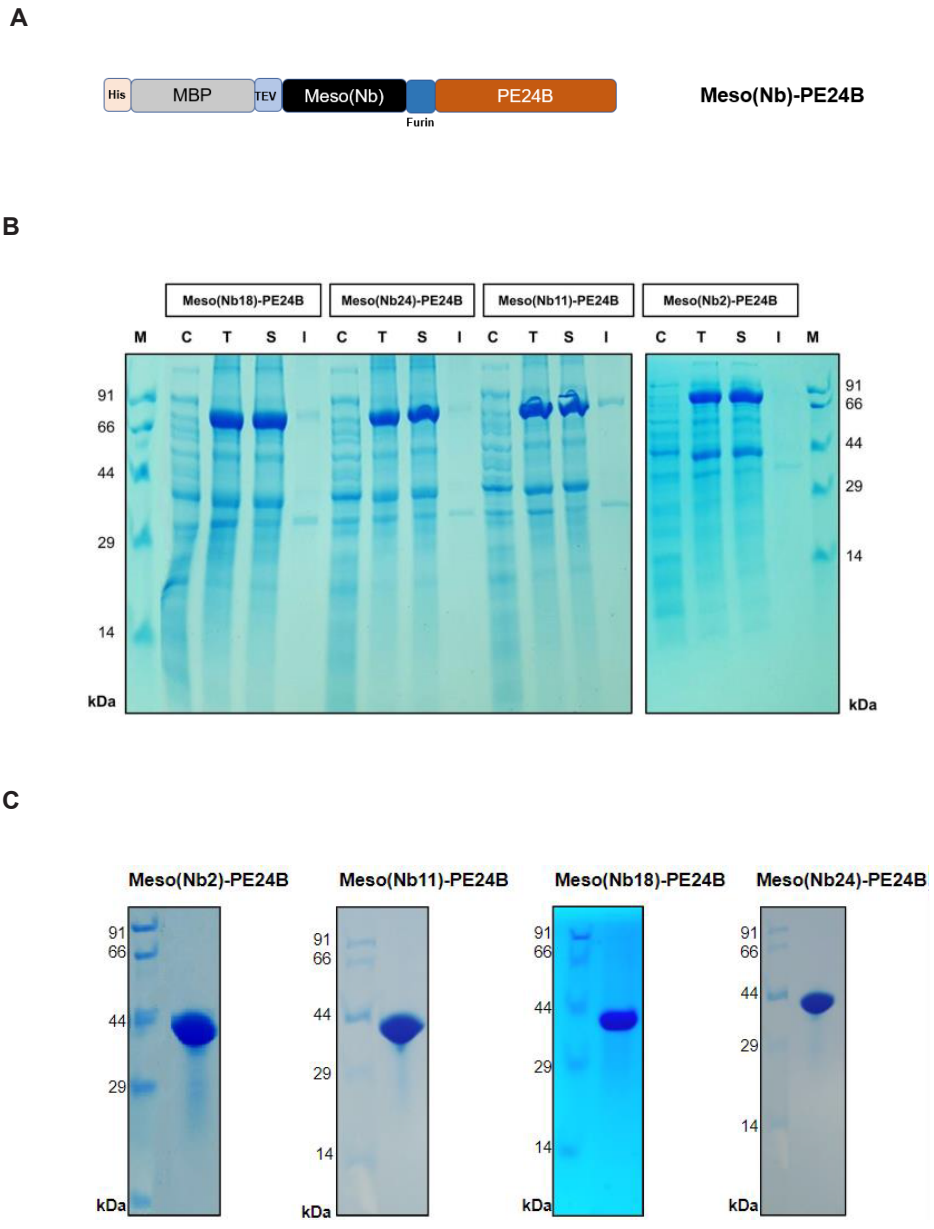

Fig. 1. Design, expression, and purification of Meso(Nb)-PE24B RITs. (A) The diagram outlines the protein architecture of Meso(Nbs)-PE24B variants. Key features include: His (histidine tag), MBP (maltose binding protein), TEV (TEV [tobacco etch virus] protease cleavage site), Meso(Nb) (mesothelin-specific nanobodies, i.e., nanobody 2, 11, 18, and 24), Furin (furin cleavage site), and PE24B (a variant of *Pseudomonas* exotoxin A). (B) Meso(Nb)-PE24B fusion proteins (variants 18, 24, 11, and 2) were expressed in the Lobstr bacterial strain at 18°C. The gel lanes are as follows: M (molecular weight marker), C (control lacking plasmid), T (total protein), S (soluble fraction), and I (insoluble fraction). Calculated molecular weights for the fusion proteins are MBP-Meso(Nb18)-PE24B: 83.35 kDa, MBP-Meso(Nb24)-PE24B: 83.53 kDa, MBP-Meso(Nb11)-PE24B: 82.92 kDa, and MBP-Meso(Nb2)-PE24B-His: 82.83 kDa. (C) All recombinant proteins were fused to an MBP tag for initial purification. Subsequent removal of the MBP tag was performed using TEV protease. Molecular weights of the purified constructs are Meso(Nb2)-PE24B: 38.83 kDa, Meso(Nb18)-PE24B: 39.35 kDa, Meso(Nb24)-PE24B: 39.53 kDa, and Meso(Nb11)-PE24B: 38.92 kDa. RITs, recombinant immunotoxins.

Table 1. Expression and solubility levels of Meso(Nb)-PE24B proteins

RITs	Expression (%)	Solubility (%)
Meso(Nb2)-PE24B	52.7 ± 5.2	98.4 ± 0.2
Meso(Nb11)-PE24B	62.4 ± 7.5	96.4 ± 0.2
Meso(Nb18)-PE24B	58.3 ± 7.4	97.6 ± 0.5
Meso(Nb24)-PE24B	60.9 ± 5.8	99.9 ± 0.4

Values are presented as mean ± SEM.
RITs, recombinant immunotoxins.
The results were derived using 1 ml from 2 L cell culture.

Table 2. The purification yield of Meso(Nb)-PE24B RITs

RITs	Amount of protein (mg)[a]	Purity (%)
Meso(Nb2)-PE24B	1.02	≥95
Meso(Nb11)-PE24B	0.76	≥95
Meso(Nb18)-PE24B	0.89	≥95
Meso(Nb24)-PE24B	1.21	≥95

RITs, recombinant immunotoxins.
[a]The results were derived from 500 ml cell culture.

RIT concentrations, the underlying cause for which remains to be determined. Conversely, minimal cytotoxic effects were observed in the HL60 promyeloblast cell line (Fig. 2C). Given these results, Meso(Nb2)-PE24B was selected for further in-depth characterization.

Characterization of Meso(Nb2) and PE24B cytotoxicities

To dissect the individual contributions of the nanobody and

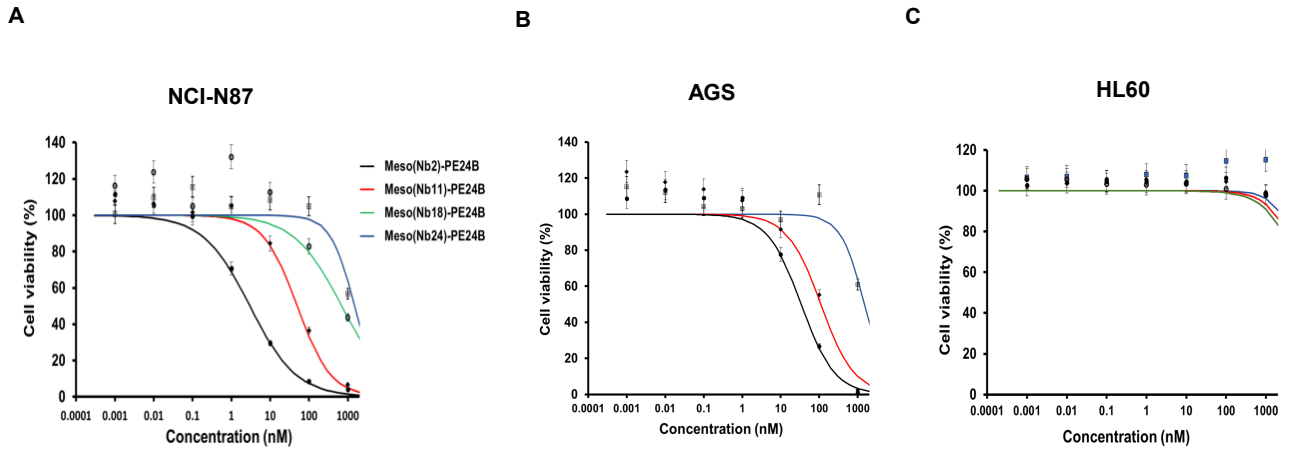

Fig. 2. Cytotoxicity profile of Meso(Nb)-PE24B constructs. Assessment of cytotoxicity for Meso(Nb)-PE24B variants on the (A) NCI-N87, (B) AGS, and (C) HL60 cell lines. Cells were exposed to RITs (0.001-1,000 nM) and incubated for 48 h. Black line (Meso(Nb2)-PE24B), red line (Meso(Nb11)-PE24B), green line (Meso(Nb18)-PE24B), and blue line (Meso(Nb24)-PE24B). RITs, recombinant immunotoxins.

Table 3. The IC_{50} and HE of Meso(Nb)-PE24B on NCI-N87 and AGS cell lines

RITs	NCI-N87		AGS	
	IC_{50} (nM)	HE	IC_{50} (nM)	HE
Meso(Nb2)-PE24B	3.9 ± 0.8	0.8 ± 0.1	33.7 ± 6.9	1.1 ± 0.2
Meso(Nb11)-PE24B	103.5 ± 18.2	1.1 ± 0.1	80.0 ± 13.3	1.3 ± 0.3
Meso(Nb18)-PE24B	≥500	0.7 ± 0.1	Not tested	Not tested
Meso(Nb24)-PE24B	≥1,000	1.4 ± 0.2	≥1,500	1.3 ± 0.1

Values are presented as mean ± SEM.
RITs, recombinant immunotoxins; HE, Hill coefficient.

toxin components to the overall cytotoxic effect, Meso(Nb2) and PE24B were separately produced and purified (Fig. 3A, Supplementary Fig. S3, Supplementary Tables S1 and S2). The N-terminal MBP of Meso(Nb2) was removed enzymatically using TEV protease during the purification process. Their biological activities were subsequently assessed across an array of cell lines, including NCI-N87, AGS, and HL60. Remarkably, Meso(Nb2) in isolation exhibited a negligible impact on cellular viability. Furthermore, PE24B alone demonstrated a cytotoxic potency that was 10 to 100-fold lower compared to the fused Meso(Nb2)-PE24B construct in the NCI-N87 and AGS cell lines (Figs. 3B and 3C, Table 4). In the HL60 cell line, cytotoxic effects were only observed at very high concentrations of PE24B (Fig. 3D, Table 4).

Generation of heterologously mesothelin-expressing cell lines

We engineered MIA PACA-2, a mesothelin-negative pancreatic carcinoma cell line, to stably overexpress mesothelin. From this, two specific cell lines—MIA/Meso-10 and MIA/Meso-18—were selected for further studies. Exposure to Meso(Nb2)-PE24B revealed a marked increase in cytotoxic potency in these cell lines, ranging from a 500- to 1,000-fold enhancement (Fig. 4, Table 5).

Internalization of Meso(Nb2) nanobody

To elucidate the internalization kinetics of the RIT within mesothelin-expressing cells, we generated a chimeric protein by genetically appending mCherry and superfolder green fluorescent protein (sfGFP) to the C-terminus of Meso(Nb2), designated as Meso(Nb2)-FP (Fig. 5A, Supplementary Fig. S3, Supplementary Tables S1 and S2). The N-terminal MBP tag was enzymatically cleaved by TEV protease during the protein purification process. The binding and internalization of this chimeric construct in MIA/Meso-10 cells were assessed via fluorescence microscopy (Fig. 5B). At the 0-h time point, both the mCherry (red) and sfGFP (green) fluorophores were prominently visible on the cell surface. Following incubation at 37°C for 2 h and 4 h, mCherry fluorescence was not only maintained at the cell surface but was also markedly observed within the intracellular compartment. Interestingly, although sfGFP was clearly visible on the cell surface, its fluorescence was not detected intracellularly. It is noteworthy that this differential pattern of fluorescence is not indicative of selective internalization but rather reflects the pH-sensitive characteristics of sfGFP (Shinoda et al., 2018). In acidic environments such as lysosomes, sfGFP loses its fluorescence, explaining its absence within the intracellular compartments after internalization. After 24 h of incubation, minimal sur-

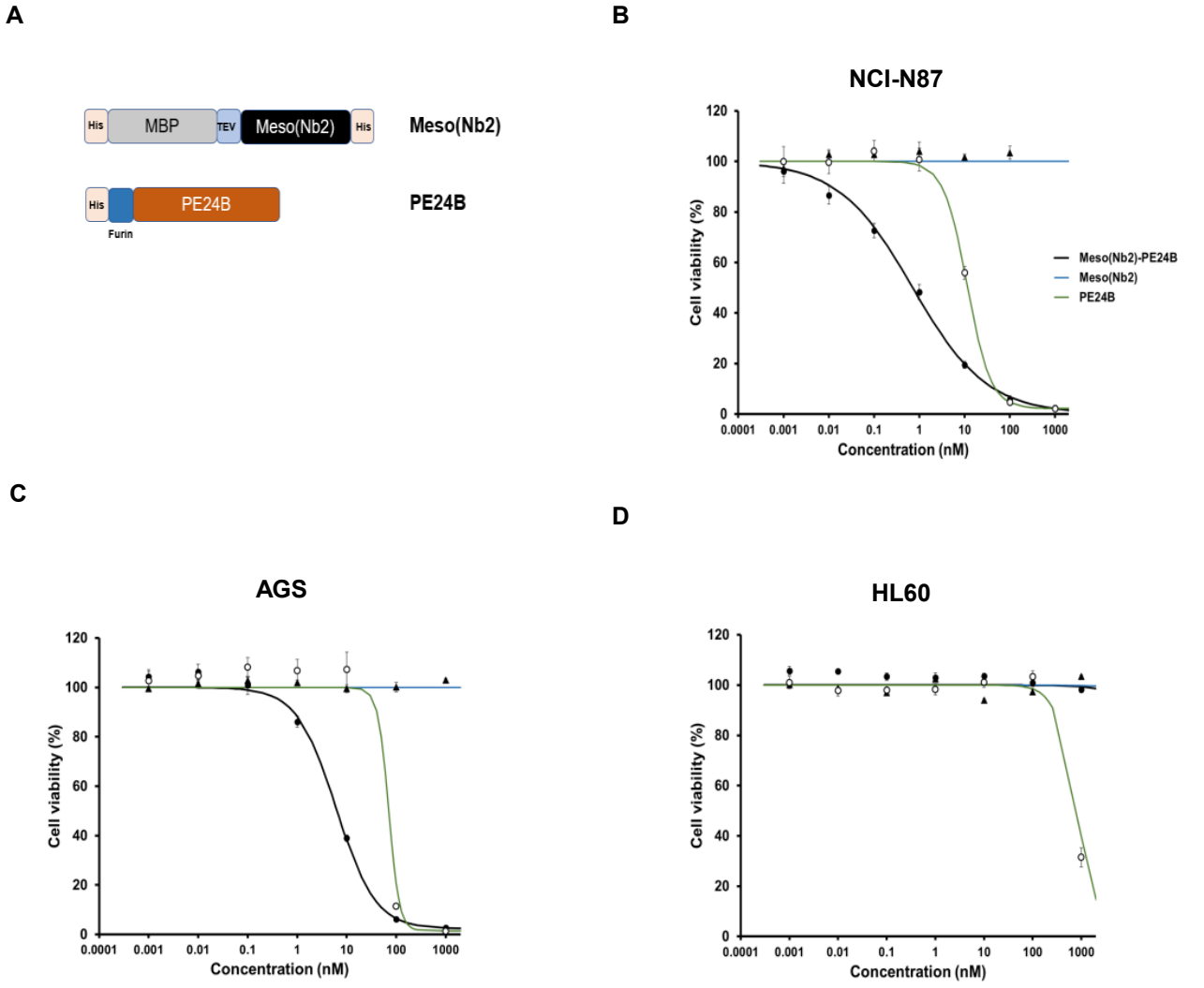

Fig. 3. Cytotoxicity assays for purified Meso(Nb2) and PE24B. (A) The schematic structure of mesothelin nanobody 2 and PE24B. His (histidine tag), MBP (maltose binding protein), TEV (TEV [tobacco etch virus] protease cleavage site), Meso(Nb2) (mesothelin nanobody 2), Furin (furin cleavage site), PE24B (a variant of *Pseudomonas* exotoxin A). (B-D) The cytotoxic efficacies of Meso(Nb2)-PE24B, Meso(Nb2), and PE24B alone were evaluated on NCI-N87, AGS, and HL60 cell lines, employing concentrations ranging from 0.001 to 1,000 nM and incubation periods of 72 or 96 h. Black line (Meso(Nb2)-PE24B), green line (PE24B), and blue line (Meso(Nb2)).

Table 4. The IC_{50} and HE of Meso(Nb2)-PE24B on NCI-N87, AGS, and HL60 cell lines

Cell line	Meso(Nb2)-PE24B		PE24B	
	IC_{50} (nM)	HE	IC_{50} (nM)	HE
NCI-N87	1.95 ± 0.50	0.54 ± 0.03	12.45 ± 0.46	1.39 ± 0.11
AGS	5.33 ± 0.88	0.90 ± 0.06	45.21 ± 3.87	2.29 ± 0.25
HL60	No effect	No effect	≥600	1.83 ± 0.22

Values are presented as mean ± SEM.
HE, Hill coefficient.

face fluorescence was detected for either fluorophore. However, only mCherry fluorescence was observed intracellularly in both the MIA/Meso-10 and NCI-N87 cell lines, consistent with the pH-sensitive properties of sfGFP, which rendered it non-fluorescent under these acidic intracellular conditions (Fig. 5C).

Evaluation of competitive binding between Meso(Nb2)-PE24B-His and Meso(Nb2)

The competitive interaction between Meso(Nb2) and Meso(Nb2)-PE24B-His for mesothelin receptor binding on mesothelin-positive NCI-N87 and AGS cell lines was investigated. Notably, Meso(Nb2) alone effectively inhibited the binding affinity of Meso(Nb2)-PE24B-His to the mesothelin receptors, as evidenced by a significant elevation in IC_{50} values for both the NCI-N87 and AGS cell lines (Fig. 6, Table 6).

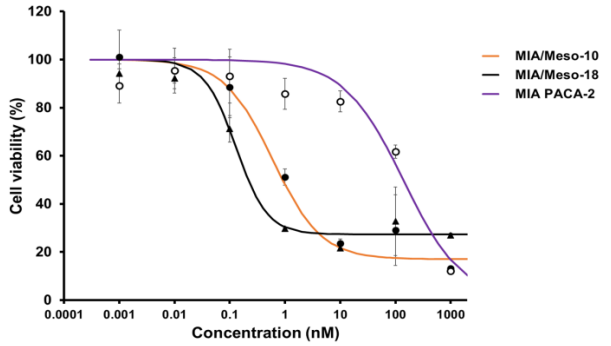

Fig. 4. Targeted cytotoxicity in mesothelin-expressing cells. Cytotoxic effects of Meso(Nb2)-PE24B on mesothelin-positive (MIA/Meso-10, MIA/Meso-18) and mesothelin-negative (MIA PACA-2) cell lines. Treatment concentrations spanned from 0.001 to 1,000 nM, with a 72-h incubation period.

Table 5. The IC_{50} and HE of Meso(Nb2)-PE24B on various cell lines

Cell line	IC_{50} (nM)	HE
MIA/Meso-10	0.62 ± 0.05	0.85 ± 0.13
MIA/Meso-18	0.17 ± 0.05	1.22 ± 0.23
MIA PACA-2	126.92 ± 9.78	0.68 ± 0.05

Values are presented as mean ± SEM.
HE, Hill coefficient.

Modification of C-terminal endoplasmic reticulum retention signal to enhance cytotoxicity

To test the effect of an endoplasmic reticulum (ER) retention signal at the C-terminus of PE24B on the cytotoxic efficacy of Meso(Nb2)-PE24B, we substituted the ER retention signal at the C-terminus of PE24B, replacing the native sequence REDLK with the more general KDEL (Fig. 7A, Supplementary Fig. S3, Supplementary Tables S1 and S2). Cytotoxicity assays performed on the NCI-N87 cell line revealed that this engineered Meso(Nb2)-PE24B-KDEL variant exhibited a 7-fold increase in cytotoxic activity (Fig. 7B, Table 7).

Cross-species reactivity and cellular binding affinities of RITs

To evaluate the cross-species reactivity and binding affinities of the RIT Meso(Nb2)-PE24B-His with respect to mesothelin in mice and monkeys, a sequence alignment was conducted. The analysis revealed an 88% homology between human and rhesus monkey mesothelins, contrasting sharply with a lower 60% homology between human and mouse mesothelins (Supplementary Fig. S4).

Meso(Nb2)-PE24B-His, engineered with a hexa-histidine tag at the C-terminus, was expressed in an eukaryotic system for assay purposes (Fig. 8A). An ELISA showed that the RITs, Meso(Nb2)-PE24B and Meso(Nb2)-PE24B-His, selectively bound to human and monkey mesothelins but not to mouse mesothelin (Fig. 8B, Table 8). Notably, the PE24B toxin itself

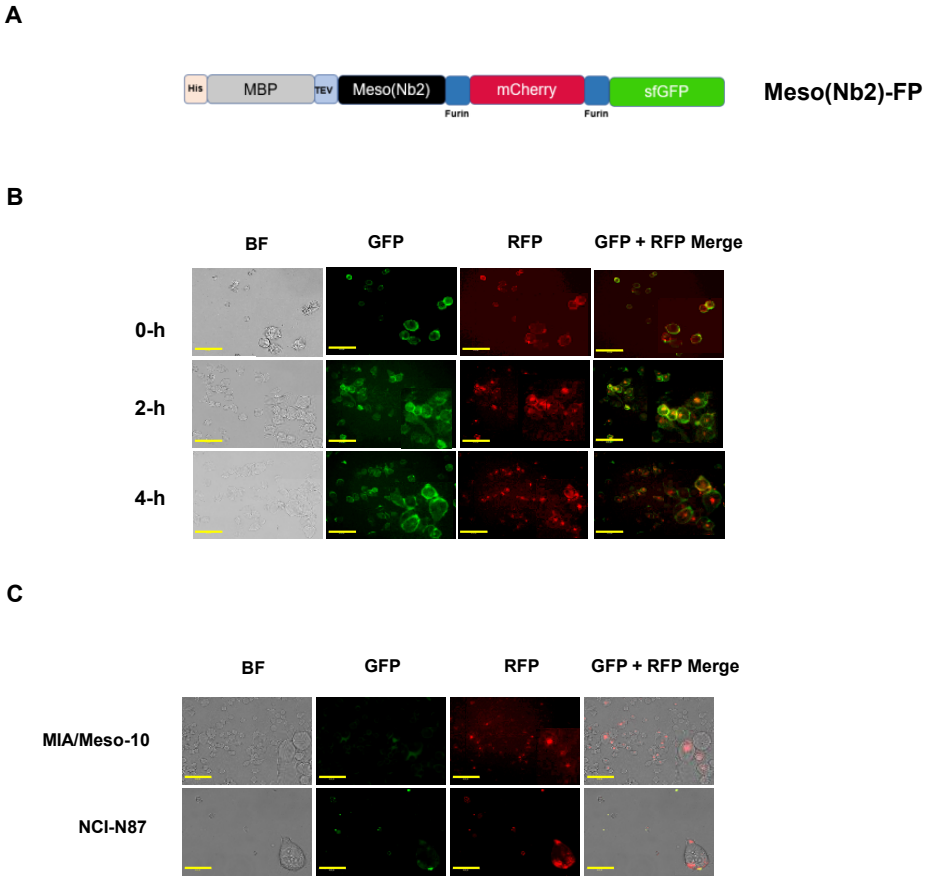

Fig. 5. Temporal dynamics of Meso(Nb2)-FP internalization. (A) Schematic representation delineates the tripartite architecture of the Meso(Nb2)-FP fusion protein, featuring mCherry as the monomeric red fluorescent protein (RFP) and sfGFP as the superfolder green fluorescent protein. (B) The internalization process of Meso(Nb2)-RP is captured in a human pancreatic cancer cell line, MIA/Meso-10, at three distinct time points visualized through fluorescence techniques. (C) The 24-h post-incubation internalization behavior of Meso(Nb2)-FP is depicted in a human pancreatic cancer cell line, MIA/Meso-10 (upper panel), and a human gastric cancer cell line, NCI-N87 (lower panel), as characterized by fluorescence. Scale bars = 100 μm. His, histidine tag; MBP, maltose binding protein; TEV, TEV (tobacco etch virus) protease cleavage site; BF, bright field; sfGFP, superfolder green fluorescent protein.

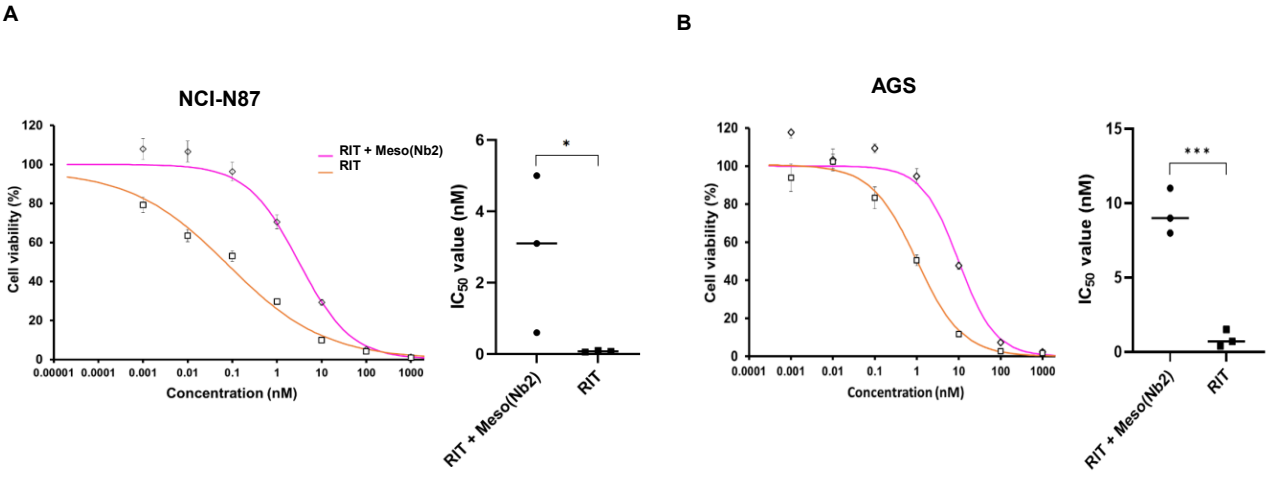

Fig. 6. The cytotoxicity of competition between Meso(Nb2)-PE24B-His and Meso(Nb2). (A) The cytotoxicity effect (left panel) and graph chart (right panel) of Meso(Nb2) alone to Meso(Nb2)-PE24B-His (RIT) on the NCI-N87 cell line. (B) The cytotoxicity effect (left panel) and graph chart (right panel) of Meso(Nb2) alone to Meso(Nb2)-PE24B-His (RIT) on the AGS cell line. Meso(Nb2) alone 100 nM added during the cytotoxic assay (n = 9, *t*-test). Orange line: cytotoxicity of Meso(Nb2)-PE24B-His (labeled as RIT in the graphical chart), pink line: cytotoxicity of Meso(Nb2)-PE24B-His supplemented with the 100 nM Meso(Nb2) fragment. RIT, recombinant immunotoxin.

Table 6. The IC_{50} and HE of Meso(Nb2)-PE24B-His on NCI-N87 and AGS cells

RITs	NCI-N87		AGS	
	IC_{50} (nM)	HE	IC_{50} (nM)	HE
Meso(Nb2)-PE24B-His	0.079 ± 0.008	0.43 ± 0.02	0.86 ± 0.23	0.8 ± 0.08
Meso(Nb2)-PE24B-His + Meso(Nb2)	2.90 ± 0.90	0.73 ± 0.11	9.33 ± 0.62	1.1 ± 0.04

Values are presented as mean ± SEM.
RITs, recombinant immunotoxins; HE, Hill coefficient.

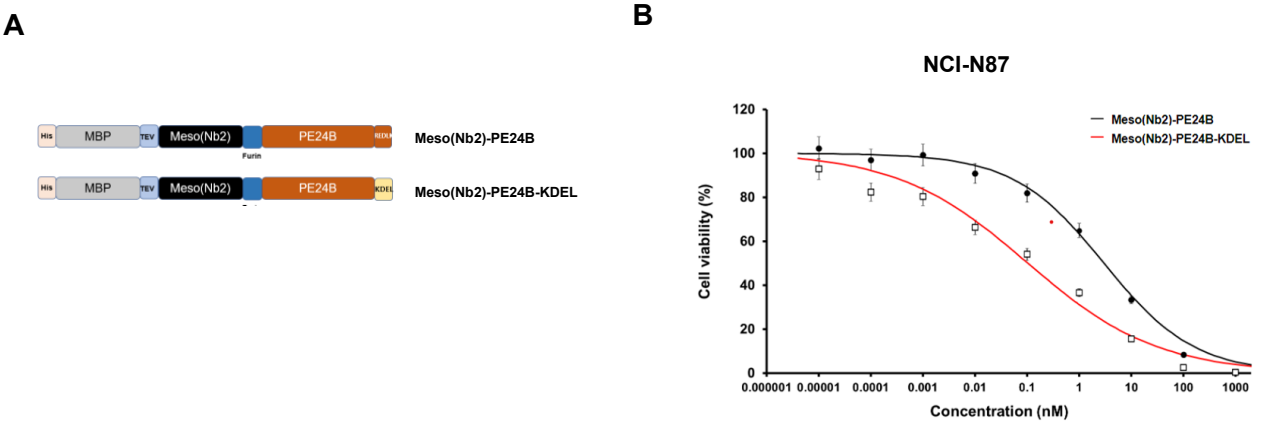

Fig. 7. Cytotoxicity augmentation by replacing C-terminal REDLK to KDEL of Meso(Nb2)-PE24B. (A) Schematic representation illustrates the molecular architecture of Meso(Nb2)-PE24B and its mutant counterpart, Meso(Nb2)-PE24B-KDEL. The native form of the molecule, Meso(Nb2)-PE24B, features PE24B-REDLK as the wild-type ER retention signal sequence, derived from a variant of *Pseudomonas* exotoxin A. Its mutant form, Meso(Nb2)-PE24B-KDEL, incorporates the modified ER retention signal sequence KDEL. (B) Quantitative assessment of cytotoxicity is presented through dose-response curves for Meso(Nb2)-PE24B (depicted in black) and its mutated form, Meso(Nb2)-PE24B-KDEL (depicted in red). His, histidine tag; MBP, maltose binding protein; TEV, TEV (tobacco etch virus) protease cleavage site; ER, endoplasmic reticulum.

did not bind to mesothelin from any of the species tested.

To further investigate the binding affinities at the cellular level, MIA PACA-2 cell lines were engineered to express monkey and mouse mesothelins, resulting in the MIA/monkeyMeso and MIA/mouseMeso cell lines, respectively. Flow cytometry analysis revealed that both Meso(Nb2) and Meso(Nb2)-PE24B-His exhibited significant binding to cells expressing human and monkey mesothelins (Fig. 8C). Noteworthy observations include stronger binding of Meso(Nb2)-PE24B-His to MIA/Meso-10 cells compared to Meso(Nb2), whereas MIA/monkeyMeso demonstrated an opposite trend. Neither of the RITs showed any binding affinity to MIA/mouseMeso or native MIA PACA-2 cells.

DISCUSSION

In the current investigation, we successfully isolated nanobodies with specificity toward mesothelin, a well-established cancer target, via high-throughput screening of a diverse nanobody library. Notably, one such nanobody demonstrated

Table 7. The IC_{50} and HE of Meso(Nb2)-PE24B-KDEL on NCI-N87 cells

RITs	IC_{50} (nM)	HE
Meso(Nb2)-PE24B	3.0 ± 0.66	0.59 ± 0.028
Meso(Nb2)-PE24B-KDEL	0.42 ± 0.28	0.43 ± 0.047

Values are presented as mean ± SEM.
RITs, recombinant immunotoxins; HE, Hill coefficient.

Table 8. K_D values of human mesothelin and monkey mesothelin

	Meso(Nb2)	Meso(Nb2)-PE24B-His
Human mesothelin	2.08 nM (R^2 = 0.998)	2.98 nM (R^2 = 0.998)
Monkey mesothelin	3.31 nM (R^2 = 0.997)	5.12 nM (R^2 = 0.995)

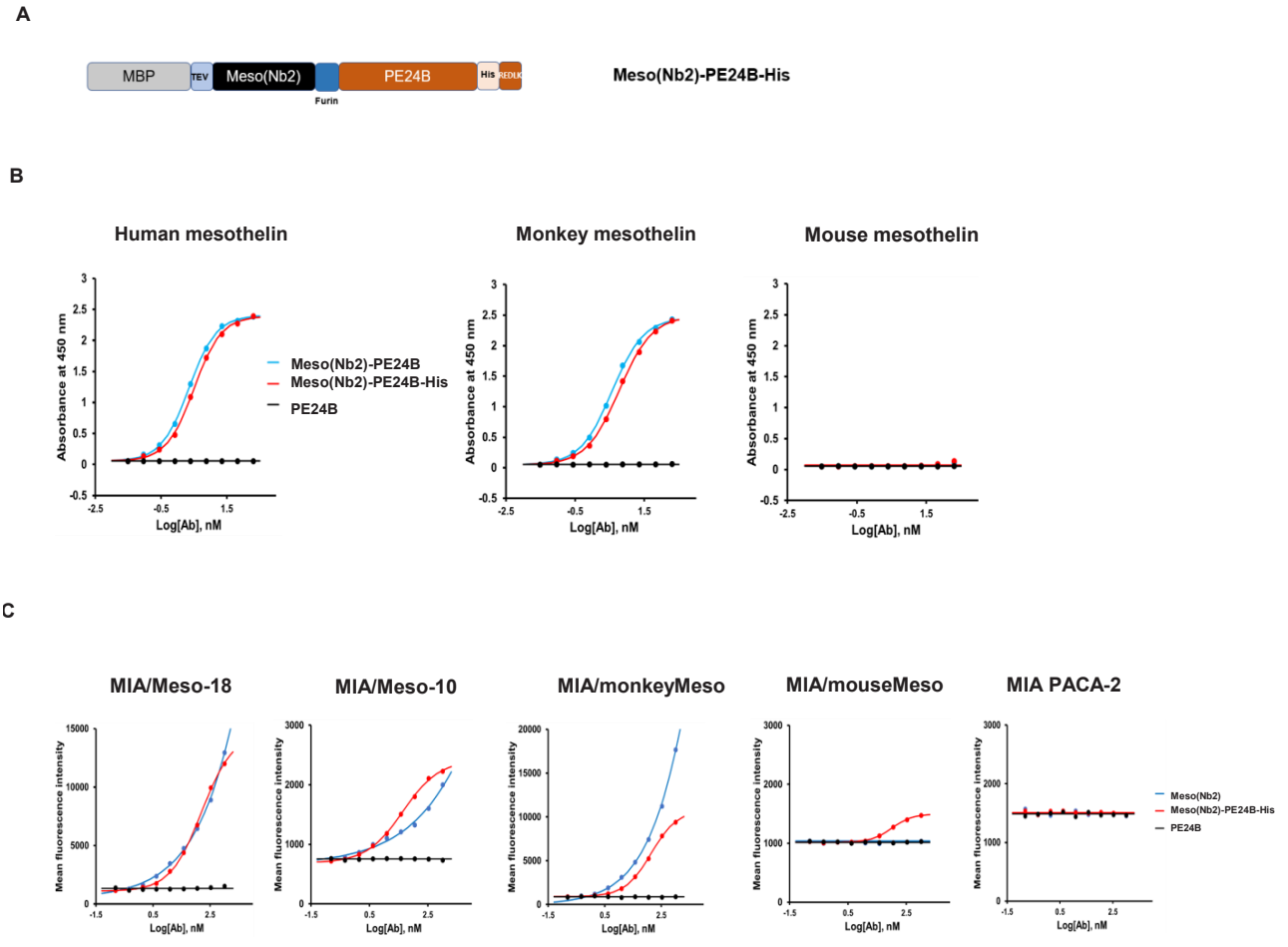

Fig. 8. Multi-species cross-reactivity and specific binding profiles of Meso(Nb2)-PE24. (A) Schematic representation delineates the architecture of Meso(Nb2)-PE24B-His fusion protein. (B) ELISA assay to assess species cross-reactivity Meso(Nb2)-PE24, Meso(Nb2)-PE24B-His, and PE24B. (C) Evaluation of specific binding of Meso(Nb2), Meso(Nb2)-PE24B-His, and PE24B on human pancreatic cancer cell lines and their engineered mesothelin-expressing counterparts using FACS (fluorescence-activated cell sorting) analysis. MBP, maltose binding protein; TEV, TEV (tobacco etch virus) protease cleavage site; His, histidine tag.

exceptional binding affinity for human mesothelin, as evidenced by an equilibrium dissociation constant (K_D) of just 2.08 nM (Fig. 8, Table 8). In the context of typical antibody affinities, which generally span from low micromolar to nanomolar K_D values, the isolated nanobody can be classified as high affinity. Future affinity maturation studies could further optimize this promising candidate into a very-high-affinity nanobody in the picomolar range. Moreover, when this nanobody was genetically fused to the PE24B toxin to create a RIT, its affinity underwent only a minimal alteration, as indicated by a slightly increased K_D of 2.98 nM (Table 8). This observation underscores the structural robustness of the nanobody, suggesting that the toxin fusion negligibly impacts its native conformation and binding capabilities.

In accordance with prior research demonstrating the advantageous role of the MBP tag in enhancing both the expression levels and solubility of recombinant proteins (Lee et al., 2019; Salema and Fernandez, 2013; Sarker et al., 2019), we successfully utilized this strategy in our study. Likewise, corroborating existing literature that identifies low-temperature induction as a robust method for augmenting protein solubility (Ferrer et al., 2004; Shirano and Shibata, 1990; Vera et al., 2007; Yi et al., 2009), we employed this approach in our experimental setup. Specifically, we engineered constructs for Meso(Nbs)-PE24B and Meso(Nb2) variants fused with the N-terminal MBP tag and subsequently expressed them in the Lobstr *E. coli* strain (Fig. 1A, Supplementary Fig. S1). Upon induction at 18°C, we achieved very good overexpression levels of the target protein. Importantly, the resultant protein exhibited an exceptionally high solubility rate, exceeding 90%, as evidenced by the data presented in Fig. 1B.

Pseudomonas aeruginosa produces the toxin PE, which is composed of three major functional domains: a receptor-binding domain, a translocation domain, and a catalytic domain (Allured et al., 1986; Siegall et al., 1989; Weldon and Pastan, 2011). Intriguingly, PE24B represents a truncated variant retaining only the catalytic domain (Hansen et al., 2010; Weldon and Pastan, 2011; Weldon et al., 2013). Conventional wisdom might suggest that PE24B should exhibit minimal cytotoxic activity, as it lacks both the receptor-binding and translocation domains that facilitate entry into cells. Contrary to this expectation, our findings demonstrate significant cytotoxic effects of PE24B in multiple cancer cell lines, including NCI-N87, AGS, and HL60 (Fig. 3, Table 4). This observed cytotoxicity is consistent with previous research that also reported substantial cytotoxic effects of PE24B in other cancer cell types, including SKBR-3, BT474, MCF7, and MDA-MB-231 (Lee et al., 2019; Park et al., 2021).

The cytotoxic mechanism of PE operates by halting cellular protein synthesis via the ADP-ribosylation of elongation factor 2, using NAD^+ as a cofactor. A specific amino acid sequence, REDLK, located at the C-terminus of PE, plays a pivotal role in directing the toxin to the ER, thereby facilitating its cytotoxic action (Chaudhary et al., 1990). Previous studies have shown that RITs that replace this REDLK sequence with KDEL—the most common ER retaining sequence—exhibit enhanced cytotoxicity (Cao et al., 2020; Kreitman and Pastan, 1995). This is likely due to improved retention within the ER, which in turn increases the likelihood of toxin translocation to the cytosol, effectively inhibiting protein synthesis. In alignment with these findings, our engineered variant that replaced the C-terminal REDLK sequence of Meso(Nb2)-PE24B with KDEL demonstrated a seven-fold increase in cytotoxic activity against NCI-N87 cells, as shown in Table 7.

We employed a chimeric fluorescent protein construct consisting of mCherry and sfGFP, fused to the C-terminus of our nanobody, Meso(Nb2). This allowed for real-time tracking of cellular internalization. Importantly, sfGFP loses its fluorescence in acidic environments such as lysosomes, while mCherry remains fluorescent, providing a useful differential signaling system (Shinoda et al., 2018). Our observations indicated that a significant amount of Meso(Nb2)-FP was internalized within 2 h, and by the 24-h mark, the majority of the fluorescently tagged nanobody had entered the cell. The mechanism of this internalization is likely mediated through receptor-mediated endocytosis (Dieffenbach and Pastan, 2020; Ecker et al., 2021; Wood et al., 2017), although further studies are needed for confirmation.

In our binding assays, the Meso(Nb2)-PE24B nanobody-toxin construct displayed strong affinity toward both human and monkey mesothelin (Fig. 8), which is consistent with the high sequence homology between these species (Supplementary Fig. S4). In contrast, negligible binding activity was observed in mouse-derived samples. This has important implications for the design of animal studies to evaluate the toxicity and therapeutic efficacy of Meso(Nb2)-PE24B. Specifically, data derived from primate models should be interpreted with greater caution compared to murine models, given that Meso(Nb2)-PE24B is capable of targeting monkey cells expressing mesothelin endogenously.

To date, alternative splicing has been shown to generate four distinct isoforms of mesothelin. One such isoform, known as soluble mesothelin-related peptide (SMRP), is predominantly found circulating in the serum (Scholler et al., 1999). Ideally, an anti-cancer agent targeting mesothelin should exhibit selective binding to mesothelin while avoiding SMRP to prevent potential interference with its therapeutic action. Both SMRP and mesothelin share sequence identity up to amino acid S592. In the mature form of mesothelin, the C-terminus is truncated, leaving S598 as the terminal amino acid, which subsequently undergoes GPI-anchor amidation. This leaves a mere six amino acids at the C-terminus of mesothelin as a unique binding epitope. Unfortunately, the mesothelin used in our library screening lacked these C-terminal six amino acids, rendering our nanobody unable to differentiate between mesothelin and SMRP. This specificity issue could be a weakness of this RIT as a mesothelin-targeted anti-cancer drug. Considering that SMRP serves as a promising serum biomarker for the early detection of malignant mesotheliomas, our nanobody may also find utility in serum-based assays for SMRP detection.

In conclusion, the present study successfully screened a high-affinity nanobody targeting mesothelin and designed, synthesized, and characterized mesothelin-targeted RITs with potent and selective cytotoxic activities. This work lays the groundwork for future investigations that may eventually lead to novel targeted therapies for mesothelin-expressing cancers.

Note: Supplementary information is available on the Molecules and Cells website (www.molcells.org).

ACKNOWLEDGMENTS
This study was supported by a grant (KNRF-2019067449) from the National Research Foundation of South Korea and by the South Korean Fund for Regenerative Medicine (KFRM) grant (RS-2023-00215312) funded by the South Korean government (the Ministry of Science and ICT, the Ministry of Health & Welfare).

AUTHOR CONTRIBUTIONS
M.Q.N. and H.C. collaborated on conceptualization, methodology, formal analysis, and manuscript preparation. M.Q.N., D.H.K., H.J.S., H.K.K.T., T.L.V., and T.K.O.N. conducted experiments and data collection, with resources provided by J.C.L. M.Q.N. curated data, and H.C. oversaw manuscript review and editing, as well as secured funding.

CONFLICT OF INTEREST
The authors have no potential conflicts of interest to disclose.

ORCID
Minh Quan Nguyen https://orcid.org/0009-0007-2554-1267
Do Hyung Kim https://orcid.org/0009-0006-0323-8171
Hye Ji Shim https://orcid.org/0009-0001-3356-6057
Huynh Kim Khanh Ta https://orcid.org/0009-0009-8417-4772
Thi Luong Vu https://orcid.org/0009-0001-9957-1342
Thi Kieu Oanh Nguyen https://orcid.org/0000-0001-6299-0191
Jung Chae Lim https://orcid.org/0000-0002-4038-9407
Han Choe https://orcid.org/0000-0003-4604-647X

REFERENCES

Alewine, C., Hassan, R., and Pastan, I. (2015). Advances in anticancer immunotoxin therapy. Oncologist *20*, 176-185.

Alewine, C., Xiang, L., Yamori, T., Niederfellner, G., Bosslet, K., and Pastan, I. (2014). Efficacy of RG7787, a next-generation mesothelin-targeted immunotoxin, against triple-negative breast and gastric cancers. Mol. Cancer Ther. *13*, 2653-2661.

Allahyari, H., Heidari, S., Ghamgosha, M., Saffarian, P., and Amani, J. (2017). Immunotoxin: a new tool for cancer therapy. Tumour Biol. *39*, 1010428317692226.

Allured, V.S., Collier, R.J., Carroll, S.F., and McKay, D.B. (1986). Structure of exotoxin A of *Pseudomonas aeruginosa* at 3.0-Angstrom resolution. Proc. Natl. Acad. Sci. U. S. A. *83*, 1320-1324.

Bird, R.E., Hardman, K.D., Jacobson, J.W., Johnson, S., Kaufman, B.M., Lee, S.M., Lee, T., Pope, S.H., Riordan, G.S., and Whitlow, M. (1988). Single-chain antigen-binding proteins. Science *242*, 423-426.

Cao, L., Li, Q., Tong, Z., Xing, Y., Xu, K., Wang, J.Y., Li, W., Zhao, J., Zhao, L., and Hong, Z. (2020). HER2-specific immunotoxins constructed based on single-domain antibodies and the improved toxin PE24X7. Int. J. Pharm. *574*, 118939.

Cerise, A., Bera, T.K., Liu, X., Wei, J., and Pastan, I. (2019). Anti-mesothelin recombinant immunotoxin therapy for colorectal cancer. Clin. Colorectal Cancer *18*, 192-199.e1.

Chang, K. and Pastan, I. (1996). Molecular cloning of mesothelin, a differentiation antigen present on mesothelium, mesotheliomas, and ovarian cancers. Proc. Natl. Acad. Sci. U. S. A. *93*, 136-140.

Chang, K., Pastan, I., and Willingham, M.C. (1992). Isolation and characterization of a monoclonal antibody, K1, reactive with ovarian cancers and normal mesothelium. Int. J. Cancer *50*, 373-381.

Chaudhary, V.K., Jinno, Y., FitzGerald, D., and Pastan, I. (1990). *Pseudomonas* exotoxin contains a specific sequence at the carboxyl terminus that is required for cytotoxicity. Proc. Natl. Acad. Sci. U. S. A. *87*, 308-312.

Dieffenbach, M. and Pastan, I. (2020). Mechanisms of resistance to immunotoxins containing *pseudomonas* exotoxin A in cancer therapy. Biomolecules *10*, 979.

Do, B.H., Ryu, H.B., Hoang, P., Koo, B.K., and Choe, H. (2014). Soluble prokaryotic overexpression and purification of bioactive human granulocyte colony-stimulating factor by maltose binding protein and protein disulfide isomerase. PLoS One *9*, e89906.

Ecker, M., Redpath, G.M.I., Nicovich, P.R., and Rossy, J. (2021). Quantitative visualization of endocytic trafficking through photoactivation of fluorescent proteins. Mol. Biol. Cell *32*, 892-902.

Ferrer, M., Chernikova, T.N., Timmis, K.N., and Golyshin, P.N. (2004). Expression of a temperature-sensitive esterase in a novel chaperone-based *Escherichia coli* strain. Appl. Environ. Microbiol. *70*, 4499-4504.

Han, S.H., Joo, M., Kim, H., and Chang, S. (2017). Mesothelin expression in gastric adenocarcinoma and its relation to clinical outcomes. J Pathol. Transl. Med. *51*, 122-128.

Hansen, J.K., Weldon, J.E., Xiang, L., Beers, R., Onda, M., and Pastan, I. (2010). A recombinant immunotoxin targeting CD22 with low immunogenicity, low nonspecific toxicity, and high antitumor activity in mice. J Immunother. *33*, 297-304.

Hassan, R. and Ho, M. (2008). Mesothelin targeted cancer immunotherapy. Eur. J. Cancer *44*, 46-53.

Ho, M., Bera, T.K., Willingham, M.C., Onda, M., Hassan, R., FitzGerald, D., and Pastan, I. (2007). Mesothelin expression in human lung cancer. Clin. Cancer Res. *13*, 1571-1575.

Huston, J.S., Levinson, D., Mudgett-Hunter, M., Tai, M.S., Novotny, J., Margolies, M.N., Ridge, R.J., Bruccoleri, R.E., Haber, E., and Crea, R. (1988). Protein engineering of antibody binding sites: recovery of specific activity in an anti-digoxin single-chain Fv analogue produced in *Escherichia coli*. Proc. Natl. Acad. Sci. U. S. A. *85*, 5879-5883.

Hyun, Y., Baek, Y., Lee, C., Ki, N., Ahn, J., Ryu, S., and Ha, N.C. (2021). Structure and function of the autolysin SagA in the type IV secretion system of *Brucella abortus*. Mol. Cells *44*, 517-528.

Jiang, Q., Ghafoor, A., Mian, I., Rathkey, D., Thomas, A., Alewine, C., Sengupta, M., Ahlman, M.A., Zhang, J., Morrow, B., et al. (2020). Enhanced efficacy of mesothelin-targeted immunotoxin LMB-100 and anti-PD-1 antibody in patients with mesothelioma and mouse tumor models. Sci. Transl. Med. *12*, eaaz7252.

Keyaerts, M., Xavier, C., Heemskerk, J., Devoogdt, N., Everaert, H., Ackaert, C., Vanhoeij, M., Duhoux, F.P., Gevaert, T., Simon, P., et al. (2016). Phase I study of 68Ga-HER2-nanobody for PET/CT assessment of HER2 expression in breast carcinoma. J. Nucl. Med. *57*, 27-33.

Khaleghi, S., Rahbarizadeh, F., Ahmadvand, D., and Hosseini, H.R.M. (2017). Anti-HER2 VHH targeted magnetoliposome for intelligent magnetic resonance imaging of breast cancer cells. Cell. Mol. Bioeng. *10*, 263-272.

Kim, S., Koh, S., Kang, W., and Yang, J.K. (2022). The crystal structure of L-leucine dehydrogenase from *Pseudomonas aeruginosa*. Mol. Cells *45*, 495-501.

Kreitman, R.J., Hassan, R., Fitzgerald, D.J., and Pastan, I. (2009). Phase I trial of continuous infusion anti-mesothelin recombinant immunotoxin SS1P. Clin. Cancer *15*, 5274-5279.

Kreitman, R.J. and Pastan, I. (1995). Importance of the glutamate residue of KDEL in increasing the cytotoxicity of *Pseudomonas* exotoxin derivatives and for increased binding to the KDEL receptor. Biochem. J. *307*, 29-37.

Lee, S., Park, S., Nguyen, M.T., Lee, E., Kim, J., Baek, S., Kim, C.J., Jang, Y.J.,

and Choe, H. (2019). A chemical conjugate between HER2-targeting antibody fragment and *Pseudomonas* exotoxin A fragment demonstrates cytotoxic effects on HER2-expressing breast cancer cells. BMB Rep. *52*, 496-501.

Liu, W., Onda, M., Lee, B., Kreitman, R.J., Hassan, R., Xiang, L., and Pastan, I. (2012). Recombinant immunotoxin engineered for low immunogenicity and antigenicity by identifying and silencing human B-cell epitopes. Proc. Natl. Acad. Sci. U. S. A. *109*, 11782-11787.

Nguyen, M.T., Koo, B.K., Thi Vu, T.T., Song, J.A., Chong, S.H., Jeong, B., Ryu, H.B., Moh, S.H., and Choe, H. (2014). Prokaryotic soluble overexpression and purification of bioactive human growth hormone by fusion to thioredoxin, maltose binding protein, and protein disulfide isomerase. PLoS One *9*, e89038.

Park, S., Nguyen, M.Q., Ta, H.K.K., Nguyen, M.T., Lee, G., Kim, C.J., Jang, Y.J., and Choe, H. (2021). Soluble cytoplasmic expression and purification of immunotoxin HER2(scFv)-PE24B as a maltose binding protein fusion. Int. J. Mol. Sci. *22*, 6483.

Prantner, A.M., Yin, C., Kamat, K., Sharma, K., Lowenthal, A.C., Madrid, P.B., and Scholler, N. (2018). Molecular imaging of mesothelin-expressing ovarian cancer with a human and mouse cross-reactive nanobody. Mol. Pharm. *15*, 1403-1411.

Roovers, R.C., Laeremans, T., Huang, L., De Taeye, S., Verkleij, A.J., Revets, H., de Haard, H.J., and van Bergen en Henegouwen, P.M. (2007). Efficient inhibition of EGFR signaling and of tumour growth by antagonistic anti-EFGR Nanobodies. Cancer Immunol. Immunother. *56*, 303-317.

Roovers, R.C., Vosjan, M.J., Laeremans, T., el Khoulati, R., de Bruin, R.C., Ferguson, K.M., Verkleij, A.J., van Dongen, G.A., and van Bergen en Henegouwen, P.M. (2011). A biparatopic anti-EGFR nanobody efficiently inhibits solid tumour growth. Int. J. Cancer *129*, 2013-2024.

Ruiz-Lopez, E. and Schuhmacher, A.J. (2021). Transportation of single-domain antibodies through the blood-brain barrier. Biomolecules *11*, 1131.

Rump, A., Morikawa, Y., Tanaka, M., Minami, S., Umesaki, N., Takeuchi, M., and Miyajima, A. (2004). Binding of ovarian cancer antigen CA125/MUC16 to mesothelin mediates cell adhesion. J. Biol. Chem. *279*, 9190-9198.

Salema, V. and Fernandez, L.A. (2013). High yield purification of nanobodies from the periplasm of *E. coli* as fusions with the maltose binding protein. Protein Expr. Purif. *91*, 42-48.

Sarker, A., Rathore, A.S., and Gupta, R.D. (2019). Evaluation of scFv protein recovery from *E. coli* by in vitro refolding and mild solubilization process. Microb. Cell Fact. *18*, 5.

Scholler, N., Fu, N., Yang, Y., Ye, Z., Goodman, G.E., Hellstrom, K.E., and Hellstrom, I. (1999). Soluble member(s) of the mesothelin/megakaryocyte potentiating factor family are detectable in sera from patients with ovarian carcinoma. Proc. Natl. Acad. Sci. U. S. A. *96*, 11531-11536.

Shahbazi-Gahrouei, D. and Abdolahi, M. (2013). Detection of MUC1-expressing ovarian cancer by C595 monoclonal antibody-conjugated SPIONs using MR imaging. Scientific World Journal *2013*, 609151.

Shinoda, H., Shannon, M., and Nagai, T. (2018). Fluorescent proteins for investigating biological events in acidic environments. Int. J. Mol. Sci. *19*, 1548.

Shirano, Y. and Shibata, D. (1990). Low temperature cultivation of *Escherichia coli* carrying a rice lipoxygenase L-2 cDNA produces a soluble and active enzyme at a high level. FEBS Lett. *271*, 128-130.

Siegall, C.B., Chaudhary, V.K., FitzGerald, D.J., and Pastan, I. (1989). Functional analysis of domains II, Ib, and III of *Pseudomonas* exotoxin. J. Biol. Chem. *264*, 14256-14261.

Song, J.A., Koo, B.K., Chong, S.H., Kwak, J., Ryu, H.B., Nguyen, M.T., Vu, T.T., Jeong, B., Kim, S.W., and Choe, H. (2013). Expression and purification of biologically active human FGF2 containing the b'a' domains of human PDI in *Escherichia coli*. Appl. Biochem. Biotechnol. *170*, 67-80.

Vera, A., Gonzalez-Montalban, N., Aris, A., and Villaverde, A. (2007). The conformational quality of insoluble recombinant proteins is enhanced at low growth temperatures. Biotechnol. Bioeng. *96*, 1101-1106.

Weldon, J.E. and Pastan, I. (2011). A guide to taming a toxin--recombinant immunotoxins constructed from *Pseudomonas* exotoxin A for the treatment of cancer. FEBS J. *278*, 4683-4700.

Weldon, J.E., Xiang, L., Zhang, J., Beers, R., Walker, D.A., Onda, M., Hassan, R., and Pastan, I. (2013). A recombinant immunotoxin against the tumor-associated antigen mesothelin reengineered for high activity, low off-target toxicity, and reduced antigenicity. Mol. Cancer Ther. *12*, 48-57.

Wolf, P. and Elsasser-Beile, U. (2009). *Pseudomonas* exotoxin A: from virulence factor to anti-cancer agent. Int. J. Med. Microbiol. *299*, 161-176.

Wood, L.A., Larocque, G., Clarke, N.I., Sarkar, S., and Royle, S.J. (2017). New tools for "hot-wiring" clathrin-mediated endocytosis with temporal and spatial precision. J. Cell Biol. *216*, 4351-4365.

Wouters, Y., Jaspers, T., De Strooper, B., and Dewilde, M. (2020). Identification and in vivo characterization of a brain-penetrating nanobody. Fluids Barriers CNS *17*, 62.

Xiang, Y., Sang, Z., Bitton, L., Xu, J., Liu, Y., Schneidman-Duhovny, D., and Shi, Y. (2021). Integrative proteomics identifies thousands of distinct, multi-epitope, and high-affinity nanobodies. Cell Syst. *12*, 220-234.e9.

Yi, A.R., Lee, S.R., Jang, M.U., Park, J.M., Eom, H.J., Han, N.S., and Kim, T.J. (2009). Cloning of dextransucrase gene from Leuconostoc citreum HJ-P4 and its high-level expression in *E. coli* by low temperature induction. J. Microbiol. Biotechnol. *19*, 829-835.

Yu, L., Feng, M., Kim, H., Phung, Y., Kleiner, D.E., Gores, G.J., Qian, M., Wang, X.W., and Ho, M. (2010). Mesothelin as a potential therapeutic target in human cholangiocarcinoma. J. Cancer *1*, 141-149.

Zhang, J., Khanna, S., Jiang, Q., Alewine, C., Miettinen, M., Pastan, I., and Hassan, R. (2017). Efficacy of anti-mesothelin immunotoxin RG7787 plus nab-paclitaxel against mesothelioma patient-derived xenografts and mesothelin as a biomarker of tumor response. Clin. Cancer Res. *23*, 1564-1574.